10 Surface Physics

T. Greber, M. Hengsberger, J. Lobo, T. Okuda, R. Schillinger, S. Berner, C. Galli Marxer, J.-H. Dil, A. Dolocan, M. Corso, C. Cirelli, M. Morscher, T. Brugger, M. Allan, S. Berner, L. Brandenberger, D. Leuenberger, T. Wassmann, T. Mattle, M. Klöckner, J. Osterwalder

The surface physics group continues to study model systems of well defined surfaces and interfaces in order to address fundamental issues that are relevant for nanoscience and nanotechnology. Our laboratory is well equipped for the preparation and characterization of clean surfaces, metal and molecular monolayer films, as well as self-assembling nanostructures, all under ultra-high vacuum (UHV) conditions. Experimental techniques available to us include x-ray photoelectron spectroscopy (XPS) and diffraction (XPD), angle-resolved photoemission spectroscopy (ARPES), two-photon photoemission (2PPE) using femtosecond laser pulses, low-energy electron diffraction (LEED) and scanning tunneling microscopy (STM). At the nearby Swiss Light Source we have built up two more photoemission spectrometers, one for spin-resolved Fermi surface mapping and one for near-node photoelectron holography. A growing network of national and international collaborations expands this set of experimental techniques and provides us also with the necessary theoretical support.

The research carried out during the report period can be grouped into three topics:

- **Electronic states at metal surfaces**
  On well ordered metal surfaces new electronic states, deviant from the bulk electronic states, arise due to the abrupt termination of the crystal lattice at the surface. These states are confined to a few atomic surface layers, while the electrons can propagate along the surface. Therefore, they can be considered as model systems for a two-dimensional electron gas. Due to the absence of inversion symmetry at the surface, spin-orbit coupling can lead to a momentum dependent spin-splitting of these states, the so-called Rashba effect. In semiconductor heterostructures, this effect represents an interesting route to manipulate electron spins by means of electric fields, thus raising a lot of interest in the field of *spintronics*. Since the splitting is much larger on these metal surface states, they permit us to study systematically how this splitting and the associated spin structures are affected by steps, kinks or adsorbates, or by regular superstructures. This is the main aim of our spin-resolved photoemission experiment COPHEE (the COmplete PHotoEmission Experiment) at the Swiss Light Source.

  Over the last years we experienced serious problems with external magnetic fields from the highly non-uniform and time-dependent magnetic environment at the synchrotron beamline entering the trajectories of the photoelectrons, leading to spurious effects in the spin-polarization measurements. We therefore decided to build an external double-walled μ-metal shield around the electron analyzer and the spin polarimeter. Designing and building this shield around the existing, highly complex instrument, represented a formidable task for our group and for the mechanical workshop (see Sec. 12). It is now finished and currently being annealed in a hydrogen atmosphere for perfect magnetic conditioning. Nevertheless, some experiments not requiring spin-polarization analysis could be performed in the meantime. As described in Sec. 10.1, a new surface state was discovered on the Ni(111) surface, for which there were some theoretical hints but so far no experimental

evidence.

- **Monolayer films of hexagonal boron nitride on metal surfaces**
  Hexagonal boron nitride (h-BN) is a layered, wide gap insulator with very strong sp^2 bonds within graphene-like sheets. Perfect single monolayers can be grown on transition metal surfaces by simple thermal decomposition of borazine, which is the BN-analogon to benzene. The study of such films has represented a large activity of the group over the last years, funded both by the SNF as well as by an EU STREP project. An important development of last year was the solution of the atomic structure of the highly complex nanomesh structure formed by h-BN on Rh(111), which could be achieved by a close collaboration within the European consortium. Rather than being a double layer structure of two incomplete mesh layers, evidence could be gathered for it being a single and complete, but highly corrugated h-BN layer (Sec. 10.2). Nevertheless, the corrugation produces a regular array of potentials wells for trapping molecules (Sec. 10.3) and small metal clusters (Sec. 10.4).

  On Ni(111), the h-BN monolayer is well lattice matched and essentially flat. This system is therefore well suited for the study of the electronic structure of this single-layer variant of boron nitride. While the occupied electronic bands have been well characterized over the last years, we were now able to perform inverse photoemission experiments at the Universität Münster in Germany in order to study also the unoccupied conduction band (Sec. 10.5), and to compare these results to our previous 2PPE results. At the same time, we extended the 2PPE measurements to high temperatures, all the way through the Curie temperature of the Ni(111) substrate, in order to establish this spectroscopy as a probe for the magnetic state of the surface (Sec. 10.6). This will give us later the opportunity to use this probe for time-resolved studies of ultrafast demagnetization of nickel by intense laser pulses with femtosecond resolution.

- **Molecular monolayers**
  By immobilizing molecules on solid surfaces we can study two types of effects. Like in a molecular crystal, we have the possibility to determine the structure of the individual molecule, which is maybe different in the adsorbed state compared to the gas phase. On the other hand, we can study the arrangement of the molecules, their interactions and the resulting electronic properties. Over the last few years, monolayers of C_{60} fullerene molecules have been one of the main scientific topics in the group. Last year, we were able to obtain unique samples of H_2@C_{60} endofullerenes from a group at Kyoto University, consisting of C_{60} buckyball cages filled with one H_2 molecule each. First photoemission experiments aiming at the electronic character of the encapsulated hydrogen molecule are presented in Sec. 10.7. Interestingly, no distinct signal due to the H_2 1σ molecular orbital is observed in the spectra.

  The electron spin is an important degree of freedom also in molecular adsorption, especially when ferromagnetic substrates are involved. The group is therefore trying to expand our instrumentation for spin polarization measurements also to the photoelectron spectrometer at the Zürich laboratory, which is equipped with excellent preparation and characterization facilities for the study of molecular layers. For this purpose, a new, simpler spin detection scheme (Sec. 10.8) is currently being evaluated.

10.1 A new surface state on Ni(111)

In collaboration with:
Peter Blaha, Institut für Materialchemie, Technische Universität Wien, A-1060 Vienna, Austria, and Luc Patthey, Surface and Interface Spectroscopy Beamline, Swiss Light Source, Paul-Scherrer-Institut, Villigen.

On Ni(111) two different surface states near normal emission are known (1; 2): an sp-band derived Shockley surface state very close to the Fermi energy with an electron-like (upward) dispersion, and a d-band derived Tamm surface state with a minimum binding energy of ∼250 meV and with a hole-like (downward) dispersion. A third surface state with Tamm character is predicted from density functional theory (DFT) calculations. It is located in the existing local d-band energy gap and originates from the deeper lying d-band. But, even though the electronic structure of Ni(111) has been studied in great detail by several groups and techniques over the last three decades, no experimental evidence for the existence of this new surface state has been produced.
To uncover this state we made use of the high sensitivity of surface states to the presence of adsorbates. Hydrogen adsorption is known to strongly affect the surface states on Ni(111), quenching them completely when the saturation coverage (∼ 0.5 ML at room temperature) is reached (3). The top graph of Fig. 10.1 shows the spectra from the clean and hydrogen saturated surface measured at normal emission with a photon energy of 35 eV. The clean surface shows a spectrum dominated by two peaks at binding energies of 0.54 eV and 1.37 eV which correspond to the bulk d-bands labeled Λ_1 and Λ_3. Two small shoulders with binding energies of 0.025 eV and 0.28 eV correspond to the Shockley and Tamm states, respectively. A first visual search for the theoretically expected new surface state is unsuccessful.

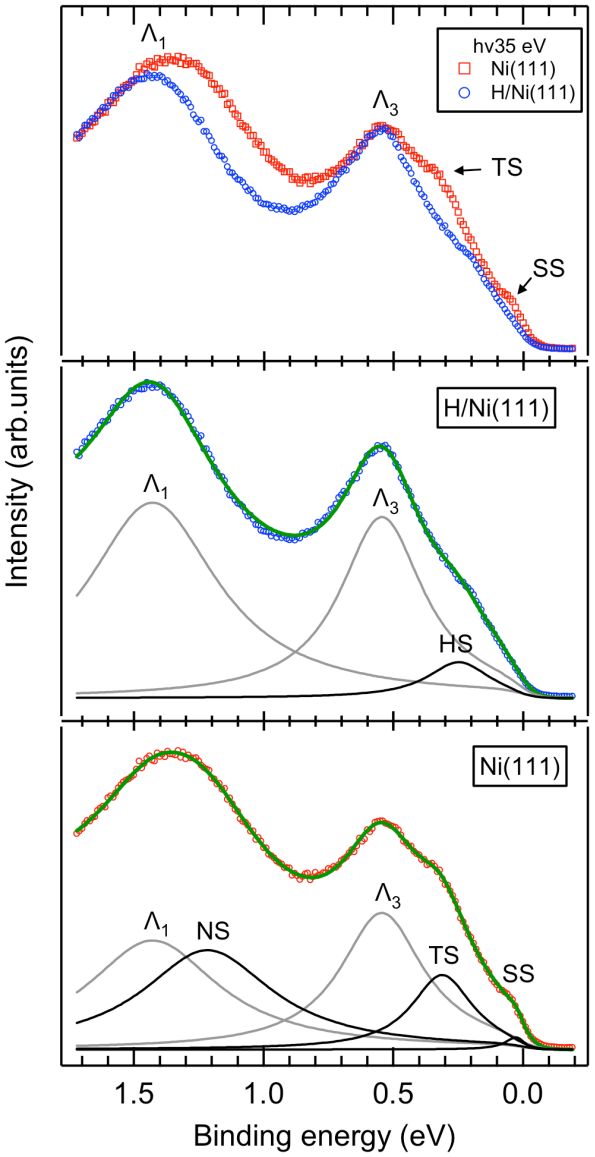

Figure 10.1: Top: Room temperature spectra measured on the clean (red squares) and hydrogen saturated (blue circles) Ni(111) surface measured at normal emission with a photon energy of 35 eV. The center and bottom panels display fits to the two spectra using a procedure described in the text. Notation: SS = Shockley state; TS = Tamm state; NS = new surface state; HS = hydrogen induced surface state; Λ_1 and Λ_3 = bulk d-bands.

The spectrum from the hydrogen saturated surface shows significant differences: the Shockley and the Tamm states have disappeared, while a new shoulder can be seen at a binding energy of 0.23 eV. Concerning the bulk states, the Λ_3 band remains basically unchanged, whereas the peak corresponding to Λ_1 experiences an ostentatious change in the peak width and an apparent binding energy shift of about 0.1 eV. This may be an indication that more than one component contribute to the Λ_1 peak. To verify this, we performed a least square fit for each spectrum assuming that both bulk bands maintain the same width and binding energy. For the clean surface spectrum, a superposition of five Lorentzian components was necessary, together with a linear background and multiplication with a Fermi-Dirac distribution. For the hydrogen-passivated surface only three Lorentzian components were needed to fit the spectrum. The overall agreement of these fits is very good. They are shown in the center and bottom graphs of Fig. 10.1. On the clean surface, the small component near the Fermi energy corresponds to the Shockley state (SS), the one found at 0.28 eV to the Tamm state (TS). The component located at 1.19 eV represents the expected new surface state (NS). It is located in the local d-band gap in between the Λ_3 and Λ_1 bulk bands, in close proximity to the latter. In this way, each of the bulk d-bands gives rise to its own Tamm surface state.

[1] F. J. Himpsel, D. E. Eastman, Phys. Rev. Lett. **41**, 507 (1978).

[2] G. Borstel, G. Thorner, M. Donath, V. Dose, A. Goldmann, Solid State Communications **55**, 469 (1985).

[3] F. J. Himpsel, J. A. Knapp, D. E. Eastman, Phys. Rev. B **19**, 2872 (1979).

10.2 Boron nitride nanomesh: a corrugated monolayer

In collaboration with:
R. Widmer and *O. Gröning*, EMPA Swiss Federal Laboratories for Materials Testing and Research, Feuerwerkerstrasse 39, CH-3602 Thun, and *R. Laskowski*, *P. Blaha* and *K. Schwarz*, Institut für Materialchemie, Technische Universität Wien, A-1060 Vienna, Austria.

Hexagonal boron nitride (*h*-BN) on the Rh(111) surface forms a highly regular hexagonal nanomesh of 2 nm pore size and a periodicity of 3.22 nm (1) which corresponds to a coincidence lattice of (13×13) *h*-BN units on (12×12) Rh lattice spacings (2). Based on STM and UPS data a first structure model was proposed, which consisted of two overlapping *h*-BN mesh layers. Further experimental studies on this peculiar material, which forms also on the Ru(0001) surface (3), and DFT calculations (4) support a new model where the nanomesh is a corrugated single *h*-BN layer. A conclusive evidence for this is given by low temperature (77 K) STM images which allow to resolve the atomic structure of the nanomesh in detail.

Fig. 10.2(a) shows a few nanomesh unit cells with a continuous hexagonal atomic lattice. The short range atomic periodicity inside the pores and on the wires has a value close to 2.5 Å (the N-N or B-B in-plane distance), and it is due to only one species within the *h*-BN layer (probably the nitrogen (5)). The large-scale nanomesh modulation appears in the rims around the mesh pores which are imaged bright even though they are topographically low, and in the inner part of the wires which are dark even though they represent the highest regions on the surface. Such electronic effects can be removed by filtering the image, thus obtaining a projection of the atomic arrangement on the surface plane (Fig. 10.2(c-d)). The nanomesh can now be viewed as formed by asymmetric hexagons,

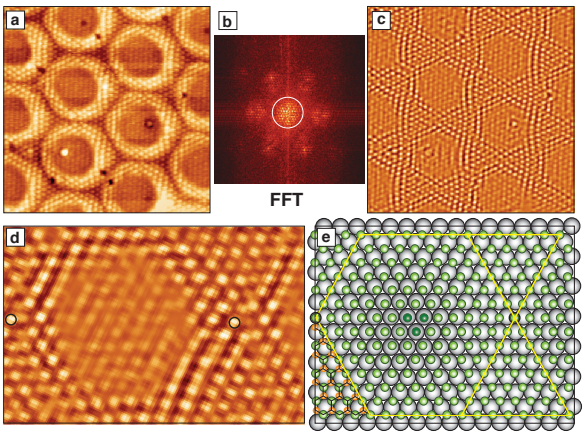

Figure 10.2:
(a) Constant current STM image (9.4×9.4 nm^2, I_t=1 nA) taken at 77 K at a sample bias voltage of V_s=-2 mV. These values are close to the Fermi level, which allows to resolve the atomic structure of the h-BN nanomesh on Rh(111). Only one atomic species is imaged. In (c), image (a) has been filtered in order to remove the 3.22 nm periodicity and to emphasize the atomic corrugation in the wires and pores. For this filtering the spots inside the white circle around the (0,0) spot in the fast Fourier transform (b) of image (a) have been removed. (d) is a zoom into (c), where a single nanomesh unit cell is enlarged permitting atom counting. In (e) a model for (d) is shown with the atomic assignment and registry given by the DFT calculations in [4]. The green atoms are nitrogen and the gray rhodium. On the bottom left of (d), some orange boron atoms are drawn to indicate the complete h-BN units. The three darker N atoms mark the center of the nanomesh pore.

the sides of which are due to alternating 6 or 7 N-N (B-B) spacings. The centers of the hexagons are represented by three atoms. Each hexagon is surrounded by six equilateral triangles with sizes defined by the corresponding side of the hexagon. Each pair of neighboring triangles shares an atom which identifies the center of the nanomesh wire. Within a single nanomesh unit cell 169 (N or B) atoms are imaged as expected for the (13×13) periodicity (Fig. 10.2(d)). The STM does not allow to make any assignment about the registry of the *h*-BN layer with respect to the substrate, since only one atomic species appears. From the DFT study by *Laskowski et al.* (4), the strongest bonding with the Rh substrate happens when the N and B atoms occupy *on-top* and *fcc* sites, respectively. In their theoretical model for the nanomesh unit cell, the pores are flat areas where the N atoms occupy nearly *on top* positions, and the BN is bonded strongly to the metal. The wires consists of two areas: in one the B atoms occupy *on-top* and the N atoms *hcp* sites, in the second one they occupy *hcp* and *fcc* sites, respectively. Since these are not optimal adsorption positions above the Rh lattice, the B and N atoms are pushed upwards by 0.55 Å, creating the topographic corrugation of the nanomesh layer. This model is in good agreement with the atomically resolved STM data (Fig. 10.2(e)), where the smaller and bigger triangles around the hexagons would correspond to the two types of wire areas. Surface x-ray diffraction experiments will be performed at the Swiss Light Source (SLS) to further refine the nanomesh unit cell structure.

[1] M. Corso, W. Auwärter, M. Muntwiler, A. Tamai, T. Greber and J. Osterwalder, Science, **303**, 217 (2004).

[2] O. Bunk, M. Corso, D. Martoccia, R. Herger, P. R. Willmott, B. D. Patterson and J. Osterwalder, J. F. van der Veen, Surf. Sci., **601**, L7 (2007).

[3] A. Goriachko, Y. He, M. Knapp, H. Over, M. Corso, T. Brugger, S. Berner, J. Osterwalder and T. Greber, Langmuir, **23**, 2928 (2007).

[4] R. Laskowski, P. Blaha, T. Gallauner and K. Schwarz, Phys. Rev. Lett., **98**, 106802 (2007).

[5] G. B. Grad, P. Blaha, K. Schwarz, W. Auwärter and T. Greber, Phys. Rev. B, **68**, 085404 (2003).

10.3 Trapping molecules in the nanomesh pores

The boron nitride nanomesh on Rh(111) (1) was used as a template to organize organic molecules on a surface. Naphthalocyanine (Nc) molecules were vapor-deposited onto the nanomesh kept at room temperature. These planar molecules have a conjugated π-electron system and their diameter of about 2 nm is comparable to the nanomesh pore size. They form a well-ordered array with the periodicity of the nanomesh (3.22 nm) as observed in the STM image shown in Fig. 10.3. High-resolution images reveal that individual Nc molecules are trapped inside the pores, indicating a highly site-selective adsorption.

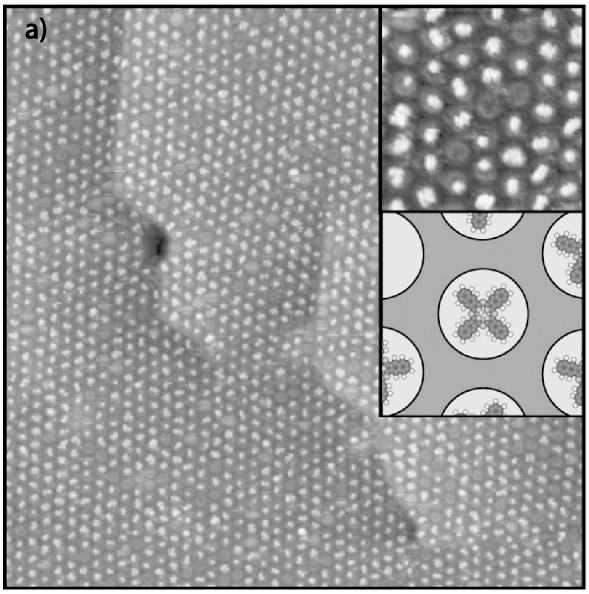

Figure 10.3: Site-selective adsorption of naphthalocyanine (Nc) molecules in the nanomesh pores. STM image (120 nm x 120 nm, I = 0.3 nA, U = 1.3 V) showing a nearly complete monolayer [3] of Nc molecules on the nanomesh. The inset on the top right shows an enlargement (19 nm x 19 nm) and gives a high-resolution view that shows the trapping of the Nc molecules inside the nanomesh pores. The inset on the right shows a schematic representation of the molecular structure of naphthalocyanine ($C_{48}H_{26}N_8$) plotted on top of a nanomesh pore.

Adding more and more molecules leads to the continuous filling of all the nanomesh pores. Molecule-substrate interactions are therefore dominating the adsorption behavior and intermolecular interactions are weak. This behavior is in contrast to Nc on flat graphite layers where the structure formation within the molecular layer is dominated by intermolecular interactions. A completely different molecular arrangement is observed in that case, with a much smaller periodicity of 1.7 nm (2).

The selective adsorption into the pores is also reflected in the normal emission UPS spectra (Fig. 10.4). The spectrum of the clean h-BN

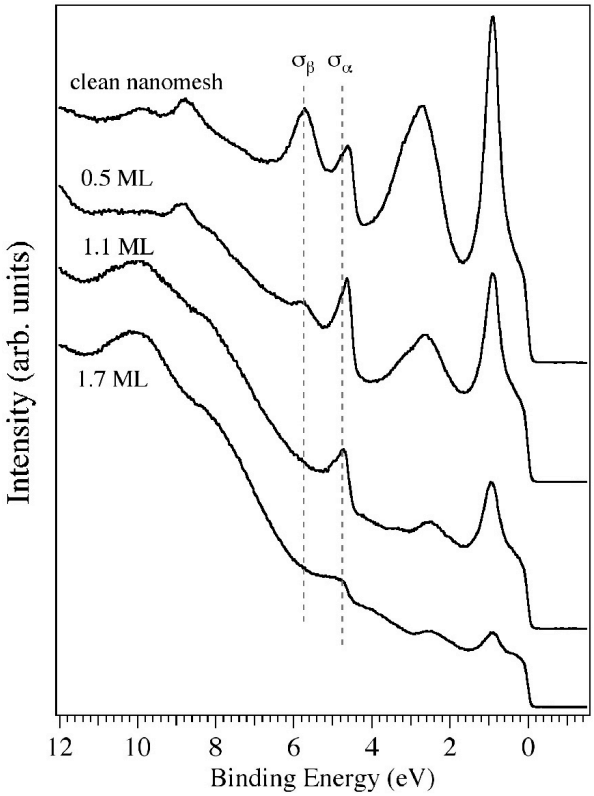

Figure 10.4: Normal emission UPS spectra for increasing Nc coverage on the nanomesh. The site-selective adsorption of the Nc is reflected in the selective attenuation up to the first monolayer of the σ_β component that is associated with the nanomesh pores. Further increasing the coverage leads also to attenuation of the σ_α component that is related to the mesh wires.

layer on Rh(111) shows the appearance of two pairs of BN-related peaks and indicates thus the presence of two species of h-BN that have their binding energies for the σ and π bands shifted by about 1 eV (1). Adsorption of the molecules onto the nanomesh leads to the attenuation of the intensity of the σ_β component, whereas the other one (σ_α) remains unchanged for coverages up to one monolayer (3) (Fig. 10.4. The σ_β component is associated with the nanomesh pores and the selective attenuation thus reflects the trapping of the Nc molecules in the pores. Further increasing the coverage leads also to attenuation of the σ_α component that is related to the mesh wires.

The strength of the trapping potential for Nc was studied in time-lapsed STM series for a partial coverage. At room temperature a very low mobility of the trapped molecules was observed with only rare hopping events. Annealing experiments confirmed the rather high diffusion barrier observed in STM. Annealing to 650 K does not lead to the desorption of the molecules from the pores. The Nc molecules thus form a robust array of equally spaced and well-separated individual molecules on the nanomesh. The present study exemplifies the potential of the nanomesh as a template for the growth of ordered molecular arrays. The large spacing between individual molecules and negligible intermolecular interactions are in many cases mandatory for preserved functionality of individual molecules on surfaces. Such arrays might be interesting for applications such as molecular electronics and storage, in photochemistry or in optical devices.

[1] M. Corso et al., Science, **303**, 217 (2004).

[2] M. Lackinger et al., J. Phys. Chem. B, **108**, 2279 (2004).

[3] The term monolayer refers in this case to one molecule per nanomesh pore.

10.4 Using the nanomesh as a template for magnetic cluster growth

In collaboration with: Philipp Buluschek and Harald Brune, Institut de Physique des Nanostructures, École Polytechnique Fédérale de Lausanne; Axel Enders and Klaus Kern, Max-Planck-Institut für Festkörperforschung, Stuttgart.

Arrays of nanometer-size particles can exhibit peculiar magnetic properties, quite different compared to the bulk properties of the same material (1). In order to investigate such differences, accurate control of the size and the arrangement of the magnetic particles is necessary. This can be achieved e.g. in metal cluster beams or through growth on supporting surfaces. We demonstrate that the h-BN nanomesh on Rh(111) (2) serves as a good template for controlled metal cluster growth.

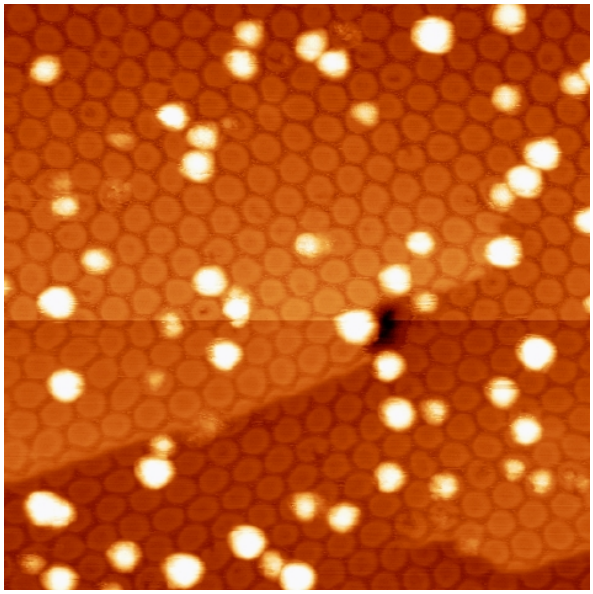

Figure 10.5: Constant current STM image of 0.1 ML Co on h-BN/Rh(111) evaporated at 300 K. Image size 50x50 nm^2, I=0.2 nA, V=0.8 V. The horizontal line near the center of the image is due to a spontaneous tip change and the associated change of tunnelling conditions. Two monatomic steps in the h-BN/Rh(111) substrate can be identified in the lower half of the image.

We evaporated cobalt (Co) onto the nanomesh at room temperature under ultra-high vacuum conditions. STM and photoemission experiments were performed to investigate the resulting morphologies and structures. STM images show that Co clusters form, with diameters comparable to the nanomesh pores. In Fig. 10.5 the result from a room temperature deposition of 0.1 ML Co, followed by a short annealing to 650 K, is imaged. At this low Co coverage the nanomesh, with its corrugation of 0.6 Å, is clearly resolved. Co clusters appear with typical heights of about 1 nm, spread randomly over the imaged area. The clusters have quite a narrow size distribution, and they are in their vast majority centered at the pores of the underlying nanomesh. This represents a first promising result regarding its functionality as a template for the growth of monodisperse metal cluster arrays.

[1] J. Shen and J. Kirschner, Surface Science **500**, 300 (2002).
[2] M. Corso et. al, Science **303**, 217 (2004).

10.5 The unoccupied band structure of h-BN on Ni(111).

in collaboration with: C. Eibl, K. Wulff, K. Zumbrägel, and M. Donath, Physikalisches Institut der Universität Münster, Germany.

In the past years, the electronic and atomic structure of a monolayer of hexonal boron nitride deposited on Ni(111) was studied in great detail with various methods (1). Some aspects, however, like the charge transfer through the boron nitride layer (2), or the reasons for the occurrence of spin-polarized photocurrents from this interface (3), strongly depend on the unoccupied band structure and cannot be studied by conventional photoemission. Two-photon-photoemission was successfully used to obtain first information about these states (4). Inverse photoemission, however, is by far the most direct way for accessing the unoccupied band structure, in particular for low photon energies (5). Briefly, a well collimated beam of monochromatic electrons is absorbed in the surface, occupying states with well defined energies and momenta. The electrons decay into states at lower energies under emission of radiation, creation of electron-hole pairs or heat dissipation. In inverse photoemission in isochromatic mode, the emission of photons within a narrow energy window (about 400 meV at 9.5 eV) is detected as a function of kinetic energy and direction of the incoming electrons. Since the photon energy and the initial electron energy are known, the final state energy inside the solid can be calculated as well as the corresponding crystal momentum. In addition, using spin-polarized electrons (6), the spin character of the bands can be extracted (7).

The measurements were carried out in the group of Prof. M. Donath at the University of Münster. The sample was a Ni(111) single crystal, which has a hexagonal frame shape such that the magnetic flux lines are closed inside the sample (7). The spectra were taken in remanence, obtained by magnetizing the sample with a current pulse through a coil wrapped around one leg of the hexagon. Spin-polarized electrons were produced using photoemission of electrons from a cesiated GaAs source using circularly polarized light (6). Some selected spectra taken from the pristine and boron nitride covered Ni(111) are displayed in Fig. 10.6. The features close to the Fermi level originate from bulk transitions (B_d) present on both samples and, in addition, from a mostly unoccupied surface state (SS) on the clean Ni(111) surface (see Ref. (7) and references therein). The image potential state (IS) found at higher energy is a bound state of an electron trapped

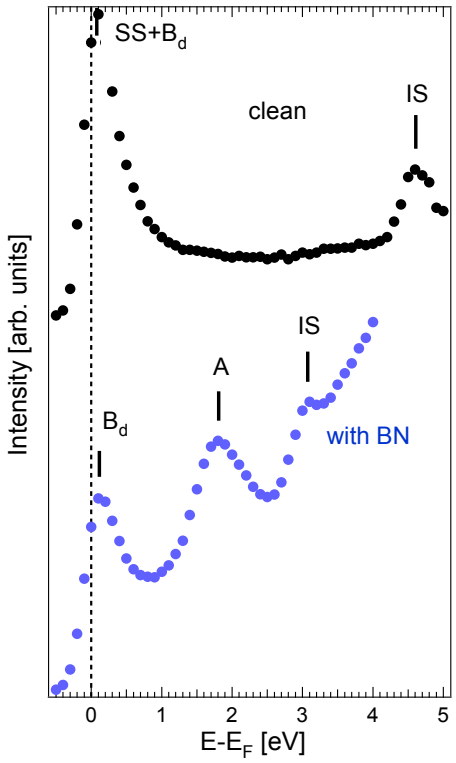

Figure 10.6: Spin-resolved inverse photoemission data from h-BN/Ni(111) in normal incidence (Θ=0°). Selected spectra from pristine and h-BN-covered Ni(111); B_d corresponds to Ni bulk states, SS to a surface transition; the interface state of boron nitride is denoted by A, the image potential states on both surfaces by IS.

between the crystal and the potential barrier of its own image potential. Its binding energy depends on the difference between Fermi and vacuum level, *i.e.* the work function. Upon adsorption of boron nitride, the work function changes dramatically by about 1.8 eV due to the modified surface dipole. Accordingly, the image state is shifted to lower binding energy by the same amount.

We focus now on the state found in normal incidence at 1.7 eV above the Fermi level, labeled A in Fig. 10.6. This state is attributed to the lowest unoccupied interface state in h-BN/Ni(111). Its energy position is in excellent agreement with density functional (DFT) calculations (1) and slightly higher than the corresponding value found in two-photon-photoemission (4). Its effective mass was found to be 1.1±0.2 in units of the free-electron rest mass (data not shown). More interestingly, theory predicts a substrate induced exchange splitting of the order of 100 meV (1). Using the asymmetry calculated from the experimental data for different directions of electron spin polarization and sample magnetization, and an instrumental spin resolution function P_{eff}, fully spin-resolved spectra can be retrieved. This is shown in Fig. 10.7 for an electron spin polarization of about 30% and a remanent sample magnetization of 70% at room temperature, as determined independently by temperature dependent measurements of the secondary electron spin polarization (8). This leads to an exchange splitting of the interface state of 150±50 meV (8), in good agreement with the DFT calculations (1). The sub-band corresponding to the spin magnetic moment aligned with the bulk magnetization direction (majority spin) is found at lower binding energy as expected from an exchange splitting

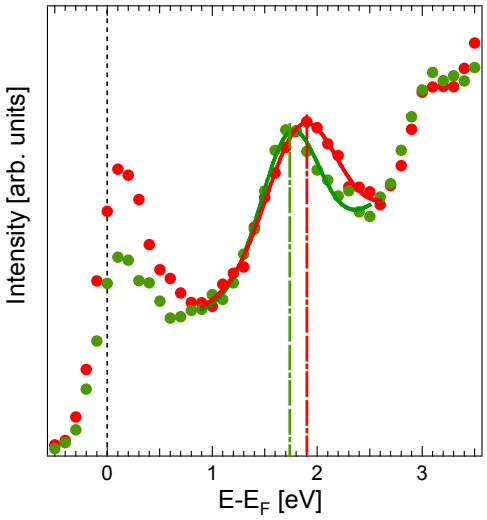

Figure 10.7:
Spin-resolved spectra, extracted from the raw data using an instrumental spin resolution function of P_{eff}≈0.2; green (red) symbols denote the spectra for spin magnetic moment pointing parallel (anti-parallel) to the bulk magnetization direction; the exchange splitting obtained in this fashion for the interface state is indicated by vertical dashed-dotted lines.

induced by the substrate magnetization. These results will shed light on the mechanism behind the spin-polarized photocurrent in particular and on spin-polarized transport through this model interface in general.

[1] G.B. Grad, P. Blaha, K. Schwarz, W. Auwärter, and T. Greber, Phys. Rev. B **68**, 085404 (2003).

[2] M. Muntwiler, W. Auwärter, A.P. Seitsonen, J. Osterwalder, and T. Greber, Phys. Rev. B, **71**, 241401 (2005).

[3] M. Hengsberger, M. Muntwiler, T. Greber, and J. Lobo-Checa,
Source for spin-polarized electrons, US patent WO 2007/006168 (published 18th of January 2007).

[4] M. Muntwiler, M. Hengsberger, A. Dolocan, H.J. Neff, T. Greber, and J. Osterwalder,
Phys. Rev. B **75**, 075407 (2007).

[5] V. Dose, W. Altmann, A. Goldmann, U. Kolac, and J. Rogozik, Phys. Rev. Lett. **52**, 1919 (1984).

[6] D.T. Pierce and F.A. Meier, Phys. Rev. B **13**, 5484 (1976).

[7] M. Donath, Surf. Sci. Rep. **20**, 251 (1994).

[8] K. Zumbrägel, diploma thesis, University of Münster, 2007.

10.6 Two-photon photoemission from h-BN on Ni(111) across the ferromagnetic phase transition

Two-photon photoemission (2PPE) is an alternative method to study the unoccupied electronic structure of surfaces, at least for states between the Fermi level and the vacuum energy. In the pump-probe mode the lifetimes of electronic excitations into such states can be measured. The method has recently been applied to h-BN/Ni(111) by our group (1). Two distinct intermediate states were detected, both populated from initial *3d*-bands of Ni(111) and with remarkably long lifetimes between 100 and 270 fs .

Nickel is considered to be the textbook example for an itinerant ferromagnet. The nonlocalized magnetic moments in nickel are carried by electrons of the spin polarized *3d*-bands, situated close to the Fermi energy. Below the Curie temperature T_c, the electrons in the completely filled *majority* subband (magnetized parallel to an external field) and from the partially occupied *minority* subband (anti-parallel alignment) are energetically separated by an amount that is termed the *exchange splitting*. As the temperature is raised, the exchange splitting is reduced and collapses completely at T_c (2). The purpose of the present study was to see how this change in the electronic structure of the ferromagnetic substrate is reflected in the 2PPE spectra from h-BN/Ni(111), where electrons from exchange-split *3d*-bands of Ni(111) are excited into intermediate states within the h-BN film before photoemission occurs by a second photon.

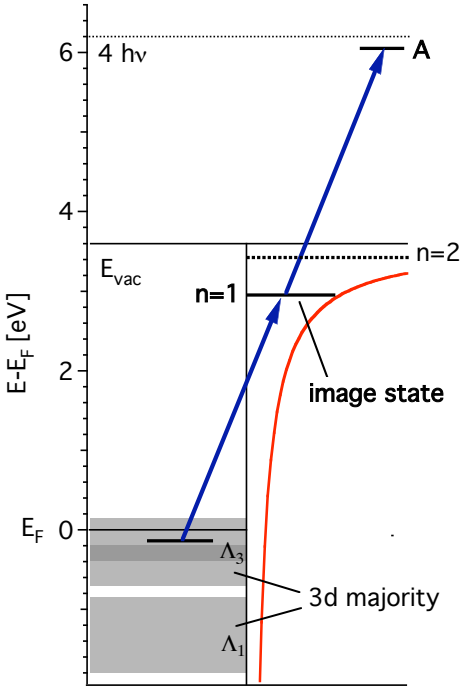

Figure 10.8: Level scheme of the blue-blue transition which is related to peak A. The red curve indicates the image potential at the Ni(111) metal surface.

Specifically, the focus was on a transition from the *3d*-bands of nickel as initial state to the unoccupied image potential state (n=1) as intermediate state, followed by a transition into a final free photoelectron state. Both transitions are induced by blue photons ($h\nu$ = 3.1 eV), provided by a femtosecond laser pulse (schematically drawn in Fig.10.8). With the aim of following the evolution of the 2PPE spectra across the magnetic phase transition of the substrate, series of 2PPE spectra were recorded while heating up and cooling down the sample surface through the critical temperature $T_c = 631$ K of nickel. The energy position as well as the width and intensity of the peak labeled A in Fig. 10.9 were monitored as a function of temperature. All of these features clearly reflect the temperature dependent magnetic phase transition of nickel at the Curie temperature.

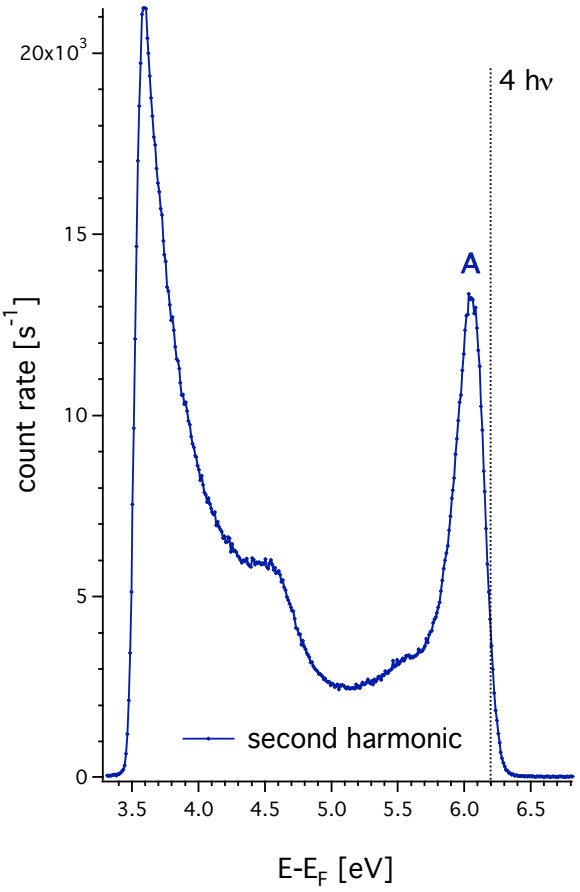

Figure 10.9: Monochromatic two-photon photoemission spectrum with blue light (hν = 3.1 eV) at normal emission and room temperature. The peak related to the image potential state is labeled with A.

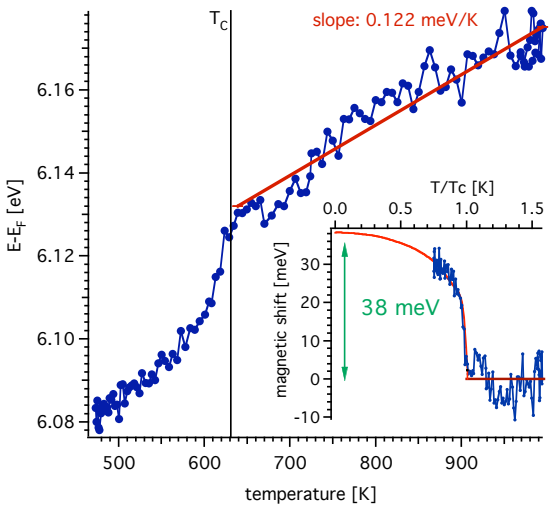

Figure 10.10: Image potential state peak position (peak A in Fig. 10.9), obtained from temperature dependent 2PPE spectra. Inset: Extracted magnetic shift of the image potential state position as a function of temperature.

Figure 10.10 shows the temperature behaviour of the peak position. Above T_c it increases linearly due to thermal lattice expansion. Below T_c, also the collapsing exchange splitting contributes to the change in peak position. Since the final photoelectron energy reflects directly the energy position of the intermediate image potential state, one can determine the exchange splitting of the (n=1) image potential state from the measured magnetic shift in Fig. 10.10. The latter can be extracted by subtracting the thermal shift from the total shift (inset of Fig. 10.10). Extrapolation to low temperatures produces a value of 38 meV which is in excellent agreement with the 2PPE study of Fischer *et al.* on clean Ni(111) that finds a value of $\Delta E_{ex} < 40$ meV at the $\bar{\Gamma}$ point in k-space (3). The investigated 2PPE image potential state transition is thereby shown to be sensitive to the ferromagnetic phase change of nickel and can thus be used e.g. to probe laser pulse induced ultrafast demagnetization.

[1] M. Muntwiler, M. Hengsberger, A. Dolocan, H. Neff, T. Greber, and J. Osterwalder,
Phys. Rev. B **75**, 07407 (2007).

[2] T. J. Kreutz, T. Greber, P. Aebi, J. Osterwalder,
Phys. Rev. B **58**, 1300 (1998).

[3] N. Fischer, S. Schuppler, Th. Fauster, and W. Steinmann,
Phys. Rev. B, **42**, 9717 (1990).

10.7 Hydrogen in C_{60}

in collaboration with: Ari P. Seitsonen, Institut de Minéralogie et de Physique des Milieux Condensés, Université Pierre et Marie Curie Paris 06, France, and Koichi Komatsu, Institute for Chemical Research, Kyoto University, Uji, Kyoto 611-0011, Japan.

Closed-cage fullerene molecules like C_{60} bear the possibility to house other atoms or molecules inside their cavity (1). This class of materials, called endofullerenes, opens many new aspects, such as the encapsulation of single atoms (1) or the chemical isolation of free electron spins (2; 3). Experiments with endofullerenes on surfaces are demanding since they ask for quantities of purified material in the micromol range, and a deposition procedure that does not affect the endohedral configuration. Recently, an organic reaction scheme, which involves the opening, filling and closing of the C_{60} cage by chemical means, was demonstrated for H_2 in C_{60}. Nuclear magnetic resonance showed H_2 to be inside the cage with a thermal stability up to 770 K (4). A hydrogen molecule inside C_{60} (Fig. 10.11) represents the simplest fullerene system housing a molecule. The volume available inside the cage corresponds to a nominal hydrogen pressure of about 1 kbar at room temperature. It is a relatively simple molecular system, though with some electronic overlap between the host and the guest molecule. Furthermore, little is known about how the peculiar spin statistics of the two protons, which dictates via the Pauli principle the population of the rotational states of H_2, is affected by the cage. Before all these interesting questions can be addressed, hydrogen represents a real challenge to be detected at all. If it can

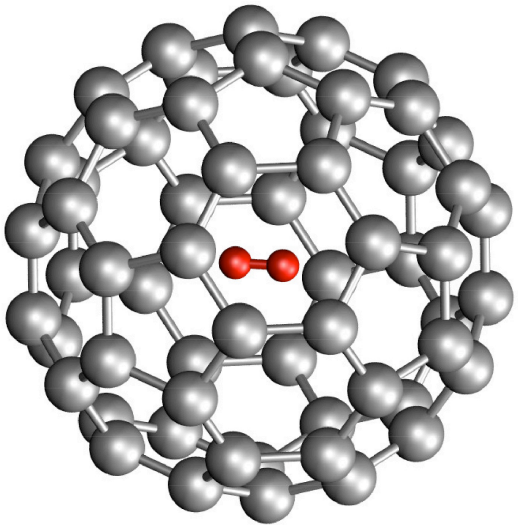

Figure 10.11:
Stick and ball model of H_2 in C_{60} (H_2@C_{60}).

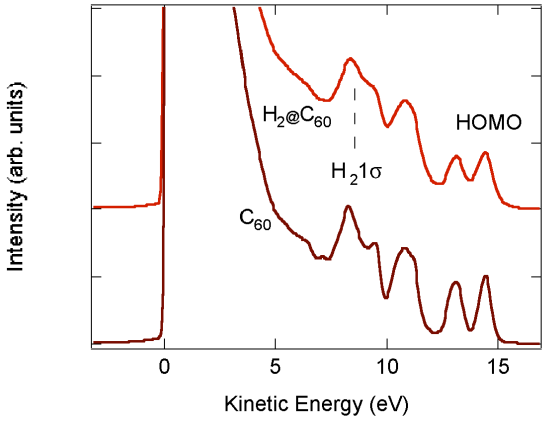

Figure 10.12: Comparison of He Iα normal emission spectra of multilayers of C_{60} and H_2@C_{60} on Al (111) recorded at room temperature. The position of the H_2 1σ molecular orbital as determined by DFT and aligned to the experimental highest occupied molecular orbital (HOMO) position is indicated as well.

be observed by photoemission, this system will give the opportunity to study issues like electron correlations and coherence in the photoemission process.

In Fig. 10.12 the photoemission spectra of multilayers of C_{60} and of $H_2@C_{60}$ are compared. The inclusion of hydrogen results in spectra similar to those of pristine C_{60}, though they are slightly less sharp. The position of the H_2 1σ molecular orbital as determined by density functional theory (DFT) for a $H_2@C_{60}$ is marked; it lies 2.76 eV above the H_2 ionisation threshold in the gas phase. This indicates that the C_{60} cage screens the H_2 1σ hole efficiently. In contrast to photoemission experiments on H_2 in the gas phase (5), no sharp H_2 1σ emission line is observed in the spectra from the endofullerenes.

[1] M. Saunders, R.J. Cross, H.A. JimŐnez-Vazquez, R. Shimshi, A. Khong, Science, **271**, 1693 (1996).

[2] T. Almeida Murphy, Th. Pawlik, A. Weidinger, M. Höhne, R. Alcala and J.-M. Spaeth, Phys. Rev. Lett. **77**, 1075 (1996).

[3] S. Yang, L. Dunsch, Chem. Eur. J. **12**, 413 (2006).

[4] K. Komatsu, M. Murata, Y. Murata, Science, **307**, 238 (2005).

[5] D.W. Turner, Phil. Trans. of the Royal Soc. of London, Series A, **268**, 7 (1970).

10.8 Test of a new electron detection scheme for Mott polarimeters

In collaboration with: Vladimir N. Petrov, St. Petersburg Technical University, Russia, and P. Robmann, Physik-Institut, Universität Zürich.

Mott polarimeters are the most widely used measurement devices to determine the electron spin polarization in photoemission experiments or in scanning electron microscopy with polarization analysis (SEMPA). These detectors exploit the left-right asymmetry in the backscattering of electrons due to spin-orbit interaction, typically from a gold foil target at electron energies of 20-100 keV. An example for an instrument using Mott detectors is COPHEE, the COmplete PHotoEmission Experiment, which has been designed and built by our group and which is now located at the Swiss Light Source. It combines angle-resolved photoemission and three-dimensional spin polarimetry by using two Mott detectors simultaneously in an orthogonal configuration (1).

The electron spin is an important but hitherto neglected degree of freedom also in molecular films on surfaces. With the purpose to implement spin resolution also in the photoelectron spectrometer in our Zürich laboratory, which offers a range of techniques for the preparation and for the characterization of molecular films, a new Mott polarimeter needs to be designed due to geometrical constraints in the existing electron analyzer. At the same time a considerable simplification of the traditional detection scheme in such detectors is attempted. The goal is to count the backscattered electrons via scintillation and to increase the maximum count rate (2). In our new design, the light pulses from the scintillators are guided through glass rods to photomultipliers outside the vacuum chamber. Therefore, the detection electronics do not need to be placed inside ultrahigh vacuum, and it can be operated at ground potential. The first tests of this detection scheme were successful. We have measured, via our light guide system, the light produced in scintillating crystals upon irradiation with electrons of energies ranging from 5 to 40 keV. A typical measurement is shown in Fig. 10.13. The resulting light yield is sufficient for a reasonable energy resolution and for noise separation at energies as low as 25 keV.

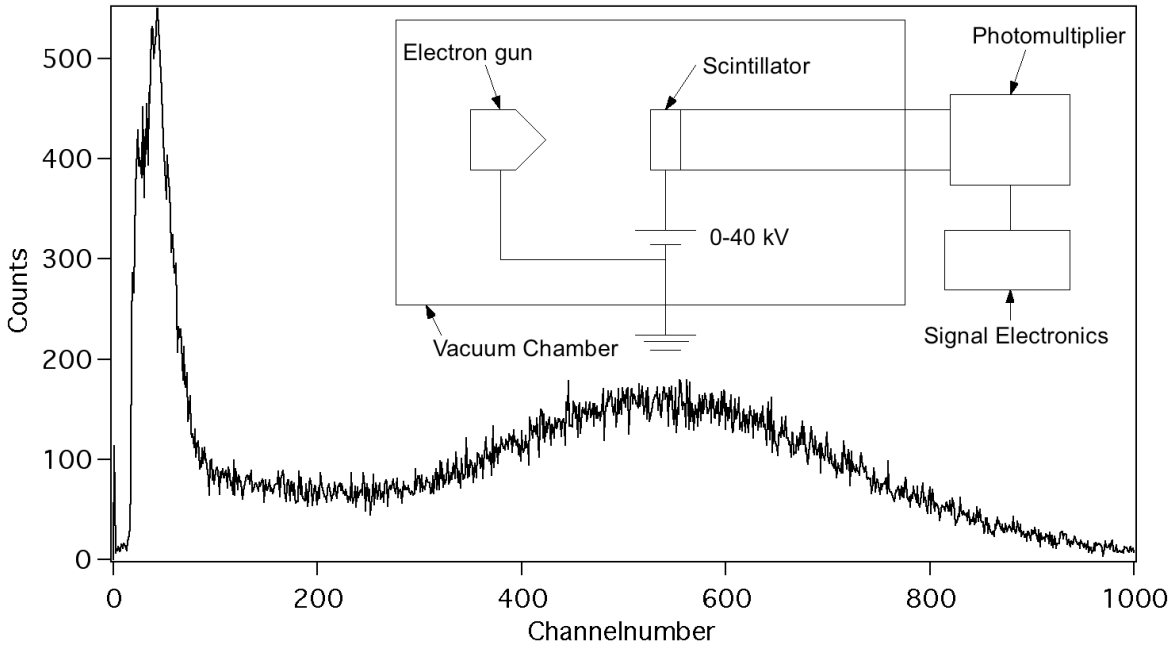

Figure 10.13: Pulse-height spectrum from the scintillator under excitation with 25 keV electrons measured with a photomultiplier. The signal due to the high-energy electrons peaks at channel 530 and is clearly separated from the contribution of single photons around channel 40. In the inset the measurement setup is shown schematically.

[1] Moritz Hoesch, PhD Thesis, Universität Zürich, 2002.

[2] V.N. Petrov, V.V. Grebenshikov, A.N. Andronov, P.G. Gabdullin, A.V. Maslevtcov, Rev. Sci. Instr. **78**, 025102 (2007).